JOURNAL OF AIRCRAFT
Vol. 45, No. 5, September–October 2008

Transition Prediction and Impact on a Three-Dimensional High-Lift-Wing Configuration

Frédéric Moens*
ONERA, 92190 Meudon, France
Jean Perraud†
ONERA, 31055 Toulouse Cedex 4, France
Andreas Krumbein‡
DLR, German Aerospace Center, 37073 Göttingen, Germany
Thomas Toulorge§
Instituto Nacional de Técnica Aeroespacial, 28850 Madrid, Spain
Pierluigi Iannelli¶
Centro Italiano Ricerche Aerospaziali, 81043 Capua, Italy
and
Peter Eliasson** and Ardeshir Hanifi††
Totalförsvarets Forskningsinstitut, 164 90 Stockholm, Sweden

DOI: 10.2514/1.36238

The evolution of the maximum-lift coefficient of a transport aircraft as a function of Reynolds number can be linked to modifications of the laminar-turbulent transition process. In the framework of European project EUROLIFT I, a task was dedicated to the physical understanding and the numerical modeling of the transition process in high-lift configurations. Then in the follow-up project EUROLIFT II, a major step was the integration of transition-prediction tools within Reynolds-averaged Navier–Stokes solvers to estimate the impact of transition on performance. This paper presents an overview of the different activities dealing with transition in the EUROLIFT II project.

Nomenclature

B, b	=	model span
C_L, C_D	=	lift and drag coefficients
C_p	=	pressure coefficient
H_i	=	incompressible shape factor
K	=	acceleration parameter for relaminarization criterion
M	=	Mach number
N_T	=	N factor at transition
P	=	static pressure
Q_e, U_e, W_e	=	total, normal, and parallel to leading-edge velocity components at the edge of the boundary layer
$\bar{R}$	=	attachment-line contamination Reynolds number
Re_C	=	Reynolds number based on reference length C
T	=	static temperature
T_u	=	external turbulence level
u, w	=	normal and parallel to leading-edge velocity components in the boundary layer
α	=	model incidence
Γ	=	intermittency function of the boundary-layer state (0 is laminar and 1 is turbulent)
δ^*, θ	=	boundary-layer displacement and momentum thicknesses
Λ_2	=	Pohlhausen parameter
μ	=	dynamic viscosity
μ_T	=	turbulent viscosity
ν	=	kinematic viscosity
ρ	=	air density
σ	=	growth rate
φ	=	sweep angle (aerodynamics), or angle between the wave number and the x direction (transition)
ψ	=	angle between the wave number and the external velocity vector

Presented as Paper 4302 at the 25th AIAA Applied Aerodynamics Conference, Miami, FL, 25–28 June 2007; received 17 December 2007; revision received 20 February 2008; accepted for publication 3 March 2008.

*Research Engineer, Applied Aerodynamics Department, Meudon Centre, rue des Vertugadins; Frederic.Moens@onera.fr. Member AIAA.

†Research Engineer, Models for Aerodynamics and Energetics Department, Toulouse Centre, Boite Postale 74025; an.Perraud@onera.fr. Member AIAA.

‡Research Scientist, Institute of Aerodynamics and Flow Technology, Bunsenstrasse 10; Andreas.Krumbein@dlr.de. Member AIAA.

§Research Engineer; currently Ph.D. Candidate, Katholieke Universiteit Leuven; Thomas.Toulorge@mech.kuleuven.be. Member AIAA.

¶Research Engineer, Applied Aerodynamics Laboratory; p.iannelli@cira.it.

**Research Leader, Division of Defence and Security, Systems and Technology; Peter.Eliasson@foi.se. Member AIAA.

††Director of Research, Division of Defence and Security, Systems and Technology; Ardeshir.Hanifi@foi.se.

I. Introduction

AIRCRAFT performance in high-lift conditions is directly related to maximum lift. An accurate estimation of this parameter early in the design process is therefore of prime importance for designers. However, most of the high-lift tests are carried out at subscale conditions and performances are then derived for flight conditions by extrapolation. But such extrapolation is only possible if the transition process is well understood in both wind-tunnel and flight conditions. Some so-called adverse Reynolds number effects may arise when comparing extrapolated results with flight-test data. For transport aircraft configurations, most of these effects are due to a change in the transition processes [1] that are Reynolds-number-dependent: Tollmien–Schlichting (TS) and

crossflow instability growths, attachment-line contamination, relaminarization, and the separation bubble.

For a clean-wing case, there may be different transition types along the span, due to changes in local conditions (local Reynolds number, pressure distribution, and flow deviation). For multi-element wings such as high-lift configurations, a similar behavior can be observed for each individual airfoil. For instance, separation bubbles may exist on the slat upper-surface, and the main wing may be fully turbulent due to attachment-line contamination, whereas transition may be triggered by TS growth on the inboard flap and by crossflow on the outboard flap.

The boundary-layer characteristics are consequently modified in a complex way, which affects the interactions existing between the different viscous layers. Therefore, computation of transition based on a turbulent pressure field is not sufficient for an accurate evaluation of the maximum lift. In particular, for a configuration equipped with a leading-edge slat device, the interaction existing between the wake of the slat and the boundary layer on the upper surface of the main wing drives the maximum lift for such a configuration [2,3].

The existence of laminar areas must be taken into account in the computation to be able to predict its impact on global performance. There are different strategies to do this coupling between transition tools and Reynolds-averaged Navier–Stokes (RANS) solvers. Most of them have been investigated within the EUROLIFT II project and were presented in previous conferences [4–6].

Turbulent computations remain useful because the major physical effects are taken into account. In addition, based on previous experiences, it has been observed that the overall turbulent pressure field obtained is very similar to the transitional one. The strong gradients at the slat or main wing leading edges tend to trip transition in the pressure recovery, and differences observed with transitional flow are visible mainly for angles of attack close to maximum lift. In the linear portion of the $C_L(\alpha)$ curve, and so for flight conditions, the assumption of a turbulent flow is therefore acceptable. This is why some activities based on the analysis of the turbulent flowfield using boundary-layer codes remain useful (in particular, for the preparation of tests) to determine the interesting locations for sensors [4], for the data analysis, or to provide realistic transition locations for computations using prescribed transition lines. In the EUROLIFT II project, an interface program has been developed by ONERA to analyze 3-D RANS computations obtained by a structured multiblock solver by a 3-D boundary-layer code, without the assumption of local 2.5-D flow usually made. This interface is not, up to now, part of an automatic coupling.

In the present paper, recent results through numerical simulation are presented on the effect of transition on the performance of a high-lift configuration, obtained in the framework of the European-Commission-funded EUROLIFT II project. In the first part, the different transition processes and their onset criteria are recalled. Then the implementation of transition-prediction tools within some computational fluid dynamics (CFD) solvers is presented and their results on different high-lift configurations are compared with those obtained using prescribed transition lines. Finally, a numerical effect of the Reynolds number on the maximum lift of a clean-wing configuration at low speed is compared with experimental data.

II. Transition and High-Lift Flows

Transition from laminar to turbulent flow may be caused by several phenomena that need to be modeled in the numerical methods. These are attachment-line contamination, short bubble transition, and transition resulting from the growth of instabilities. Relaminarization must also be considered because it may appear downstream of contamination.

A. Attachment-Line Contamination

Attachment-line contamination is due to the transport of fuselage (or wind-tunnel floor) turbulence along the attachment line of the wing. Increased sweep and large curvature radius in the attachment-line region promote this transport. When this occurs, the whole wing surface becomes turbulent, with no laminar region. Attachment-line contamination is characterized by the parameter

$$\bar{R} = W_e \Big/ \sqrt{\nu \left(\frac{\partial U_e}{\partial X}\right)_{X_a}}$$

with X_a referring to the attachment line. It can be shown to vary as the square root of the Reynolds number, or of the nose radius, and increases with sweep. The critical value [7,8] of the $\bar{R}$ parameter is usually taken as 250 ± 20.

In the case of an infinite-swept-wing assumption, calculation of $\bar{R}$ first requires the knowledge of the effective sweep angle φ_{eff}, from which $W_e = Q_\infty \sin(\varphi_{\text{eff}})$ is obtained. An iterative method may be used for this purpose, looking for a linear evolution with distance to the attachment line of the normal to leading-edge velocity $U_e = \sqrt{Q_e^2 - W_e^2}$. A similar approach can be used for conical wings.

In the case of direct extraction from the RANS field of the velocity components, $\bar{R}$ can be determined from the velocity gradient at the attachment line, which may usually correspond to a mesh point. Alternatively, it is possible to detect attachment-line contamination by means of the attachment-line momentum-thickness Reynolds number Re_θ, which can be estimated with the help of pressure and geometry data. It has been shown from similarity solutions on the attachment line that criteria on Re_θ and $\bar{R}$ are equivalent: $Re_\theta = 0.404\bar{R}$.

B. Relaminarization

One of the characteristics of the high-lift configurations is the strong pressure gradients at the upstream elements (slat and main wing). Strong acceleration of a turbulent flow may damp the production terms, to a point that the flow returns to a seemingly laminar state: this is called relaminarization. In 2-D flows, the acceleration parameter

$$K = \frac{\nu}{U_e^2}\frac{\partial U_e}{\partial x}$$

proposed by Beasley [9] is a local parameter, which can be obtained in the preprocessing step, together with attachment-line transition Reynolds number $\bar{R}$. In 3-D flow, K should be evaluated in the streamline direction. Relaminarization of a turbulent boundary layer should be expected if values of K are larger than 5×10^{-6} over a significant distance. Large values have the effect of keeping the boundary layer in a quasi-laminar state, called *laminarescent* [10], but as soon as K decreases, the turbulence reappears rapidly.

Return to turbulence proceeds as in a bypass transition, without going again through a linear stage. Laminar separation of a laminarescent flow may be observed. A turbulent flow is required upstream of relaminarization, as may be caused by contamination.

C. Transition from Growth of Instabilities

In the case of a three-dimensional base flow, transition may be triggered due to two different processes, based on the growth of instabilities: the first is based on the streamwise component of the velocity (longitudinal waves) and the second is based on the crossflow profiles. Transition will occur as soon as one of the two reaches a sufficient level. These different processes have been modeled inside boundary-layer codes for many years, either through transition criteria or through models known as *database methods*.

1. Criteria

The longitudinal criterion requires the computation of the incompressible shape factor $H_i = \delta^*/\theta$. The Arnal–Habiballah–Delcourt (AHD) criterion [11] was developed for the prediction of longitudinal transition caused by TS and oblique instabilities linked to the streamwise component of the velocity profile. This criterion, based on the same parameters as the Granville criterion, was developed from linear stability analysis of self-similar incompressible velocity profiles ($H_i < 2.7$). The Mack relation $N_T = -8.43 -$

$2.4\,\ell_n(T_u)$ provides the link between the transition location and the external turbulence level. The criterion writes $R_{\theta_T} - R_{\theta_{cr}} = f(T_u, \bar{\Lambda}_2)$, where

$$\bar{\Lambda}_2 = \frac{1}{x_T - x_{cr}} \int_{x_{cr}}^{x_T} \frac{\theta^2}{\nu} \frac{dU_e}{ds}\, ds$$

is an averaged Pohlhausen parameter, $R_{\theta_{cr}} = \exp(52/H_i - 14.8)$ defines the so-called critical location (the end of the stable region), and

$$f(T_u, \bar{\Lambda}_2) = -206 \exp(25.7\bar{\Lambda}_2)[\ell_n(16.8T_u) - 2.77\bar{\Lambda}_2]$$

This criterion was recently extended to compressible flow.

Transition due to crossflow instabilities is predicted by means of the C1 criterion [11], based on the crossflow displacement thickness δ_2. Note that δ_2 is usually better estimated in a RANS approach than in a boundary-layer code, because its evaluation does not suffer from the lasting effect of initialization of this parameter in boundary-layer codes. The C1 criterion is defined with

$$R_{\delta_{2_T}} = \frac{300}{\pi} \tan^{-1}\left(\frac{0.106}{(H_i - 2.3)^{2.052}}\right)$$

where

$$\delta_2 = \int_0^{\delta} -\frac{w(y)}{U_e}\, dy$$

2. Models

Another approach, developed at ONERA and referred to as the database method [12,13], provides an estimation of the growth rate σ of a 2-D compressible boundary layer directly from mean flow parameters and the boundary-layer profile characteristics. The starting idea is that the Reynolds number variation of growth rates obtained solving the exact Orr–Sommerfeld equations can be represented for a given profile using two half-parabolas:

$$\sigma = \sigma_M \left(1 - \left(\frac{R_{\delta 1} - R_M}{R_k - R_M}\right)^2\right) \qquad \begin{matrix} R_{k=}R_0 & \text{if } R_{\delta 1} < R_M \\ R_{k=}R_1 & \text{if } R_{\delta 1} > R_M \end{matrix}$$

This parabola model (Fig. 1) requires the determination of R_0, R_1, R_M, and σ_M as functions of nondimensional frequency

$$F = \frac{2\pi f \nu}{U_e^2}$$

boundary-layer characteristics and mean flow conditions. These functions were established from sets of exact stability solutions of Falkner–Skan self-similar profiles in compressible 2-D flows. The first model was thus created for longitudinal instabilities based on a lookup table using the values of the incompressible shape factor H_i and the local Mach number M_e.

Crossflow instabilities are inflectional in nature: they are determined by the location and characteristics of the velocity profile inflection point. Considering 2-D similar profiles with reverse flow, it was shown that two parameters allow representing the Reynolds dependence of the growth rate: $U_i = u(y_i)$ and $P_i = y_i(\partial u/\partial y)_{y_i}$, where y_i is the location of the highest inflection point. A purely

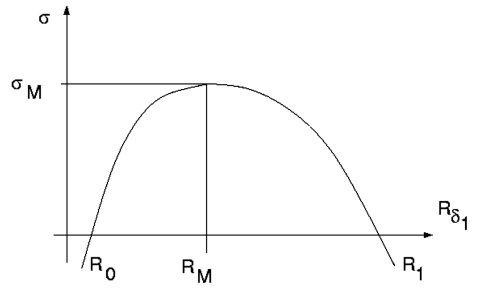

Fig. 1 Growth-rate variations represented using parabolas.

analytical model was built for this purpose, first considering attached Falkner–Skan profiles and later extended based on typical compressible profiles close to the leading edge of a transonic wing. For 3-D profiles, Stuart's theorem, as described in [14], states that in temporal theory, the growth rate σ_ϕ in any direction ϕ can be determined from the stability of the 2-D velocity profile projected in the ϕ direction of the original 3-D profile. The projected profile is defined as $U_\Phi = (v/k)U + (\beta/k)W$ $(k = \sqrt{v^2 + \beta^2})$, with the reduced frequency $F = 2\pi f v/U_\Phi^2$, Gaster's relation [15] then provides a relation from temporal to spatial growth rates.

The two models, for longitudinal and for crossflow instabilities, were later combined into a single model. The resulting database method for transition prediction allows an estimation of the stability characteristics of 3-D boundary layers with high efficiency. Growth rates obtained are integrated to produce envelope N factors exactly as in the case of exact stability theory. Careful optimization has ensured that, in general, the most amplified frequencies are represented with an error below 10%.

D. Separation

For 2-D short bubble transition, the Gleyzes–Habiballah criterion [16] can be applied. It uses an analytical representation of the amplification curves for 2-D Falkner-Skan similar profiles with reverse flow ($H_i > 2.7$). For these profiles, stability results are almost independent of frequency but mostly depend on the incompressible shape factor. Hence, N-factor evolution can be written as

$$N(s) - N(s_1) = \int_{R_{\theta_1}}^{R_\theta} \frac{-2.4}{G(H_i)}\, dR_\theta$$

where $G(H_i)$ is an analytical expression of only H_i, and $N(s_1)$ is the total growth rate at location s_1, where $\theta = \theta_1$. $N(s_1)$ can be obtained using the AHD criterion. Transition is assumed to occur when $N(s) = N_T$, given by Mack's relation. In the course of EUROLIFT II, AHD and Gleyzes–Habiballah criteria were combined into a single criterion by ONERA using the same estimation procedure for the incompressible shape factor as a function of the Pohlhausen parameter [17]. An automatic detection of separation is used in the elsA code to select the proper model for longitudinal transition.

In the framework of EUROLIFT II, a subtask was dedicated to the characterization of three-dimensional separation bubbles on a single airfoil to obtain some estimation of changes in the characteristics of boundary layers due to variation of the transition point.

The flow case studied here is the ONERA-D symmetrical airfoil at low speed ($M_0 = 0.15$, $Re_c = 0.810^6$) with a leading-edge sweep $\varphi = 60$ deg. The angle of attack in a plane normal to the leading edge is 8 deg. The transitional RANS computations were performed by ONERA using the unified AHD/Gleyzes criterion for 2-D bubbles. In computations, the transition point, where Γ growth from 0 to 1, is found at $x/c = 0.0945$. In this case, laminar separation was found starting at $x/c = 0.013$ (upstream of the transition point) and reattachment was at $x/c = 0.47$. The data are compared with those of a fully turbulent computation (which does not exhibit any flow separation).

Figure 2 presents the corresponding computed streamlines. The boundary-layer characteristics are presented in Fig. 3 (in the laminar, transitional, and turbulent parts of the flow) based on the velocity profiles extracted from the RANS solutions. It can clearly be seen that the boundary layer for the separated flow is remarkably thicker than that for the fully turbulent case, even in the laminar part of the separation bubble. Additionally, a sensitivity study to transition location was carried out using a Totalförsvarets Forskningsinstitut (FOI) interactive boundary-layer code. The flow case corresponds to the ONERA-D case but with lower outer streamwise velocity. The main characteristics of the tools used by the Instituto Nacional de Técnica Aeroespacial (INTA), DLR, German Aerospace Center (DLR), and ONERA are described hereafter.

As the transition point in the computations moves from $x/c = 0.05$ to 0.16, the height of the recirculation zone increases dramatically by a factor of about 3, and the boundary-layer thickness at the trailing edge is nearly multiplied by two, but because the

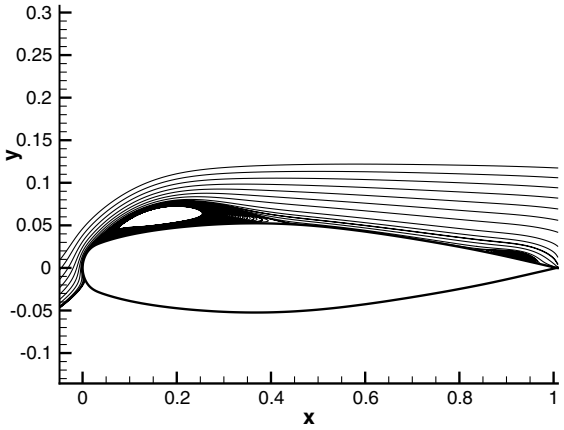

Fig. 2 Computed separation bubble on the ONERA-D airfoil; $M_0 = 0.15$, $\alpha = 8$ deg, $Re = 0.8 \times 10^6$, and $\phi = 60$ deg.

transition point is located inside the separation bubble, the separation point is almost unaffected (Fig. 4). The computation of laminar separation bubble is therefore highly sensitive to the location of the transition point and to the way turbulence is introduced.

E. Specificities of High-Lift Configuration Flowfields

The high complexity of the flow existing over a high-lift multicomponent wing is shown in Fig. 5. The main characteristics can be summed up as follows:

1) Locally compressible flow (possibly slightly supersonic) in the slot gaps and at the leading edge for high angles of attack is embedded into dominantly incompressible low Mach numbers ($M_0 \sim 0.15$ to 0.25).

2) The significant effect of viscous flows (separations and wake/boundary-layer interactions) drives the absolute level of performance (lift, drag).

3) The multicomponent wing implies different local Reynolds numbers (local chord variation) and varying sweep angles with the spanwise location.

4) Different transition mechanisms may exist at the same time on each element.

Some so-called adverse Reynolds number effects may be observed on maximum-lift evolution with Reynolds number, which can be partly related to a change in the transition process (Fig. 6). For instance, for a clean-wing configuration equipped with a throughflow nacelle tested in the framework of EUROLIFT I, experimental results have shown a constant increase in maximum lift when Reynolds number increases, up to a certain critical Reynolds number at which $C_{L\max}$ decreases. The analysis of the pressure distribution for $M_0 = 0.20$ has shown that the critical Reynolds number on $C_{L\max}$ corresponds to a change between transitional and fully contaminated cases (Fig. 7). Even if the direct link between maximum-lift evolution and change in transition process is not established, the coincidence makes this possibility somewhat probable.

Therefore, taking the effects of transition into account in the design process is considered to be necessary for a precise prediction of performance. This can be done either experimentally by using a pressurized cryogenic wind tunnel such as the European Transonic Wind Tunnel (ETW) facility to reach the flight flow conditions or done numerically by introducing transition effects into CFD methods. Different strategies for doing so are presented in the next section.

III. Different Levels for Taking Transition into Account

A. Level 0: Turbulent Computation and Boundary-Layer Analysis

This methodology is often used to have an estimation of the boundary-layer characteristics, including the transition location. This information can be used for test preparation, for the identification of interesting areas for measurements, and for locating the sensors. For instance, the preparation of the Aile à Flèche Variable (AFV) tests in the EUROLIFT I project considered this procedure [4] (see Sec. IV for the test-case description).

Classical weak coupling is based on an Euler calculation of the mean flow followed by a boundary-layer computation. Iterative correction of the Euler flow may be important because there is no viscous layer in the Euler flow. In the case of a weak coupling

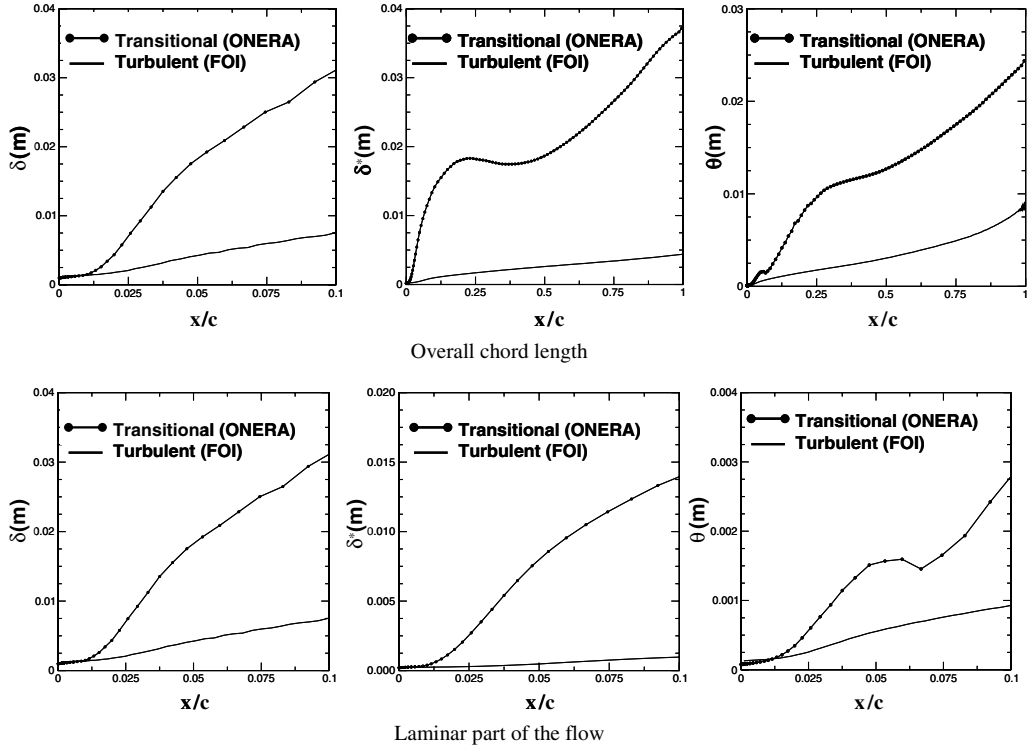

Fig. 3 Evolution of the boundary-layer characteristics for turbulent and transitional computations.

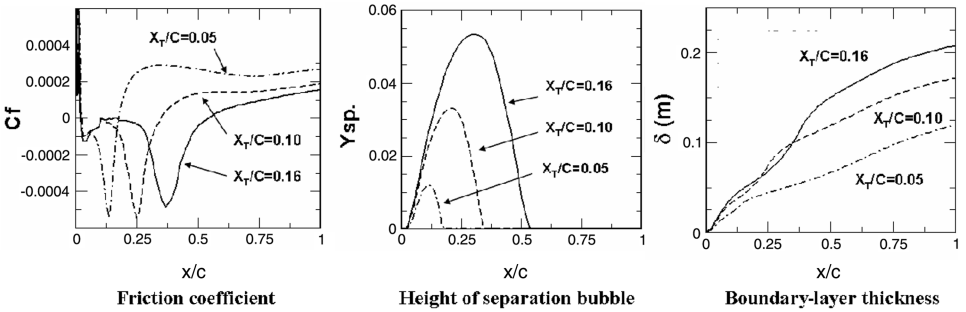

Fig. 4 Influence of the prescribed transition point in the computations on the bubble characteristics.

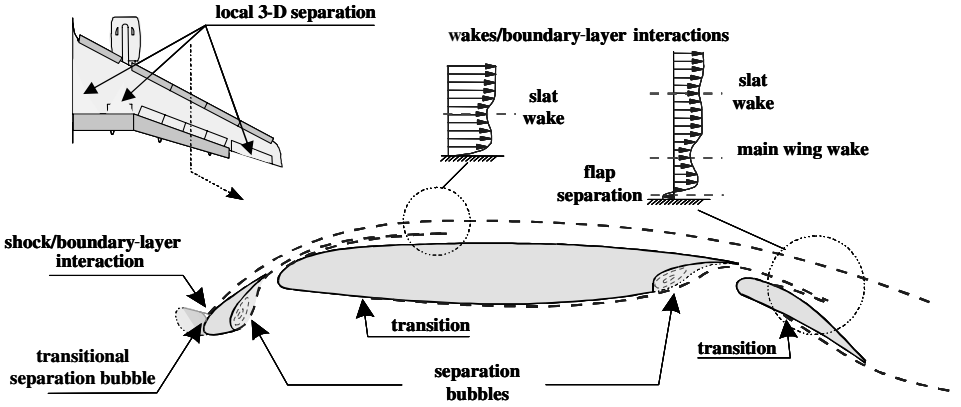

Fig. 5 High-lift-flow main characteristics.

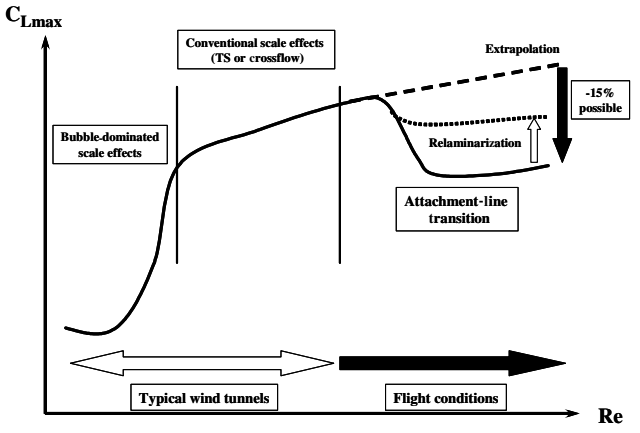

Fig. 6 Scheme of adverse Reynolds number effect on $C_{L\max}$ and possible link with changes in transition process.

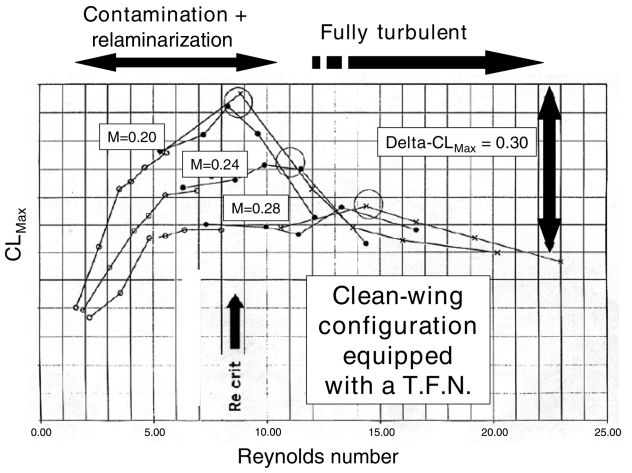

Fig. 7 Analysis of experimental data: possible link between evolution of $C_{L\max}$ and change in transition process on a clean-wing configuration equipped with a nacelle (T.F.N. denotes a throughflow nacelle).

between a RANS field and a boundary-layer code, this iterative correction is less critical because there is a boundary layer in the RANS field. From experience, one-step weak coupling may be used to generate an estimation of the boundary-layer evolution, including transition. Even without iterative correction of the mean flow, this procedure remains commonly used for high-lift configurations, because it was frequently observed that the force coefficients and pressure distributions are not significantly modified by changing the Reynolds number in the linear portion of the $C_L(\alpha)$ curve, but differences occur near maximum lift. In addition, it has to be used to check whether or not transition occurs on the attachment line.

However, a number of questions need to be considered when extending such an approach to complex 3-D configurations. First, the local external velocity components, mandatory for most of the boundary-layer codes, must be determined from the RANS flow. Second, special care must be taken when boundary layers interact with viscous wakes with different flow directions. In the framework of EUROLIFT II, ONERA has developed such an interface [18] and evaluated different sensors. In addition, a suitable mesh for RANS computation is often not adapted for boundary-layer codes. In particular, a grid perpendicular to the leading edge is generally preferred for boundary-layer codes, whereas grids are often generated considering constant spanwise location for RANS solutions.

Finally, for the boundary-layer characterization, two approaches can be used:

1) Consider selected wing sections and assume the flow to be locally 2.5-D and then interpolate the transition line between two sections. This process is the most frequently used.

2) Consider a 3-D evaluation of the boundary layer directly.

It must also be noted that this procedure can be considered as the first step for a coupling between CFD solvers and boundary-layer codes for the development of a numerical tool that can deal with automatic transition-prediction capabilities.

B. Level 1: Prescribed Transition Line

The next step in the method to take transition into account in CFD codes is one of the most frequently used. Based on experimental results or from analysis carried out using the previous level, using a level-0 analysis, the transition location is known at some wing sections. Then a linear evolution between two sections, or a constant-x/c location, is assumed for the transition location. Computations are then carried out by imposing the eddy viscosity to zero in the laminar part. Strictly speaking, this method is rather laminar-area-imposed instead of taking into account the transition. It must also be noted that the way laminar areas are imposed in the solver could lead to nonphysical specification of laminar/turbulent regions in the flowfield. As an illustration, Fig. 8 presents the way laminar extents have been imposed in the Centro Italiano Ricerche Aerospaziali (CIRA) solver (corresponding to the case $\alpha = 12$ deg). It can be seen, for instance, that by using such an approach, a nonphysical wake issued from the slat is computed. The slat wake starts turbulent, then becomes laminar, and then turbulent again. Though the slat gap/overlap of such configurations appear to be large enough to avoid any strong downstream interaction between the slat wake and the main wing near-wall boundary layer, such an unphysical wake development could lead to more important deficiencies in the aerodynamic performance prediction of more generic configurations. It is therefore recommended to limit the area in which turbulent viscosity is set to zero to an extension slightly higher than the boundary-layer thickness.

C. Level 2: Computed Transition Lines

The CFD tools used for high-lift-flow prediction in the industry are mainly RANS solvers. In general, this kind of solver does not feature any specific transition simulation capability: they only rely on turbulence models to estimate the Reynolds stress tensor in the whole computational domain. In recent years, several attempts to include laminar-turbulent transition prediction within RANS computations in a more or less automatic way have been carried out. They can be classified into three approaches.

The first approach is to use low Reynolds number turbulence models [19] or special transition/turbulence models [20]. Although it is a very natural way to implement transition-prediction capabilities into RANS solvers, this approach cannot model the various physical phenomena related to transition.

The second approach, recently proposed by Langtry and Menter [21], consists of using transport equation models for the intermittency and some special variable that tracks transition (e.g., momentum-thickness Reynolds number Re_θ). The solution of these equations defines the laminar and turbulent regions. It thus mimics the effects of transition (in a recent version, the Re_θ function seems to be able to correlate with TS-type transition) without modeling its internal physics. The implementation of such a method in RANS solvers is fairly natural and applies to any kind of mesh and geometry. However, it still lacks a correlation for transition triggered by instabilities, particularly of crossflow type, as well as a leading-edge contamination correlation, which are significant transition mechanisms in high-lift flows.

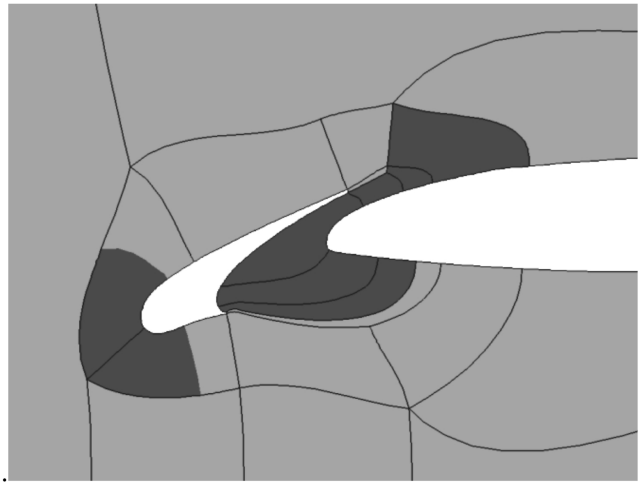

Fig. 8 Example of laminar areas prescribed in a RANS computation leading to an unrealistic slat wake; laminar (dark) and turbulent (light).

The third approach involves the use of a transition-prediction method inside the RANS code. The goal is to compute the transition location within the RANS calculation and to control the turbulence by means of the effective viscosity $\mu_{\text{eff}} = \mu + \Gamma \mu_T$, where μ is the classical laminar dynamic viscosity, μ_T is the turbulent eddy viscosity, and Γ is an intermittency function. In the laminar region, $\Gamma = 0$, and at the detected transition location Γ should rise to simulate the start of turbulence; the simplest example is the step function. With this approach, a frequent evaluation of the transition location is necessary to ensure the compatibility of the flow with the imposed laminar/turbulent state during the iterative convergence process. Hence, a requirement for the transition detection method is a low computational cost, which does not advocate for full linear stability analysis or parabolized stability equation methods in complex cases. In this context, two ways have been explored.

1) The first way consists of using transition criteria to predict the occurrence of either TS or crossflow transition. A number of local (only using boundary-layer local parameters and wall normal gradients) and nonlocal criteria were evaluated at ONERA for use within a RANS code.

2) The second way consists of using database e^N methods based on linear stability theory to detect transition; the velocity profiles in the boundary layer, required to perform the stability analysis, can then be obtained in two manners. The first procedure is to extract the velocity data directly from the RANS mesh [22]. This method has been shown to require a high grid resolution in the boundary layer, especially for the prediction of crossflow transition [22,23]; at the moment, this is not compatible with the requirements on computational effort for industrial 3-D applications. The second procedure to obtain high-resolution velocity profiles is to compute them with a boundary-layer code [24,25]. Here again, several approaches are possible, which were explored in the framework of the European EUROLIFT projects. The input data for the boundary-layer computation may be the RANS surface pressure, in which case a hypothesis of an infinitely swept [26] or conical wing [27] needs to be used. Alternatively, the input data can be directly extracted from the 3-D velocity field, allowing the coupling to a 3-D boundary-layer code.

To date, the most reliable predictions for 3-D flows could only be obtained with the third approach (transition-prediction methods inside RANS codes), because it is the only approach able to model the main natural transition mechanisms on smooth swept wings: namely, TS and crossflow instabilities. In addition to natural transition predicted by criteria or the e^N method, three other phenomena are important in the context of high-lift flows: leading-edge contamination, relaminarization, and transition through a separation bubble. They occur because of very large pressure gradients observed around the slat and main wing leading edges, leading to strong accelerations, but they remain difficult to insert in automatic prediction tools, as they are very sensitive to threshold values. Up to now, these phenomena have been evaluated separately.

The different tools using internal transition-prediction capabilities used in the EUROLIFT II project belong to this third approach, with some variants in the way transition lines are computed. The main characteristics of these different tools are described hereafter.

1. *INTA's Tool*

For the tool used by INTA, the chosen strategy is the coupling of a RANS solver with an e^N method through a boundary-layer code,

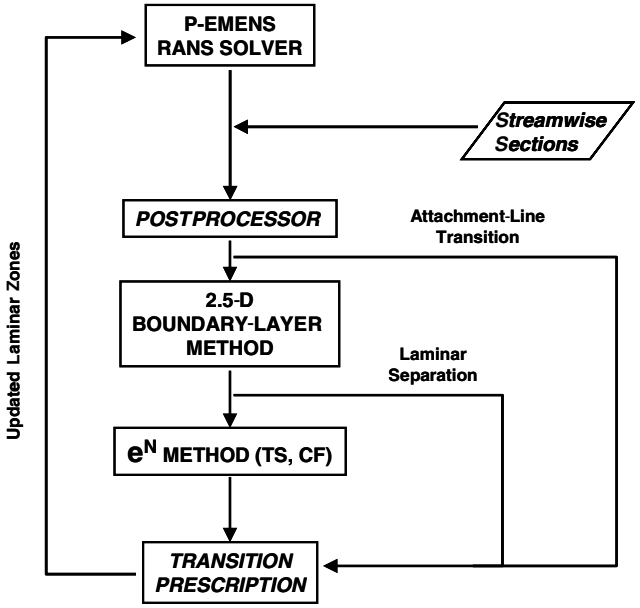

Fig. 9 General strategy used for transition prediction in INTA's tool (CF denotes crossflow).

based on the local 2.5-D approach. The general strategy retained for the INTA tool is illustrated in Fig. 9.

The solver used for Navier–Stokes computations is the P-EMENS code developed by Airbus Spain and EADS-CASA and improved by INTA. It solves the RANS equations by means of a finite volume discretization, the value of the unknowns being cell-centered on structured multiblock meshes. Time is being integrated by means of Runge–Kutta schemes, featuring various techniques for convergence acceleration to steady state (local time stepping, multigrid). The RANS equations can be closed either by the k-g or by Spalart–Allmaras/SALSA turbulence models. The transition-prediction tool is based on a 2.5-D approach: the boundary layer is computed and analyzed in several sections of the configuration, and the resulting transition locations are interpolated to the 3-D RANS computational domain. From these results, it becomes possible to prescribe transition in the RANS code for a new computation, thus iterating the whole cycle until convergence. Under-relaxation (with respect to the preceding cycle iteration) is usually applied on the prescribed transition location to prevent it from moving too far upstream, in which case the real transition point would be unrecoverable.

The module handles point transition; intermittency is represented by a step function. One of the main assumptions consists of considering that laminar separation immediately triggers transition if no instability is detected upstream. Moreover, attachment-line contamination is considered to take place in sections where $Re_\theta \geq 100$ on the attachment-line and the attachment-line momentum-thickness Reynolds number Re_θ can be estimated with the help of only pressure and geometry data [28]. The boundary-layer submodule is the Kaups–Cebeci procedure [27] to solve the compressible laminar boundary-layer equations, assuming local conical flow and taking the value of the pressure at the wall as input boundary-condition data. The resulting velocity profiles feed the stability analysis module that consists of the e^N database method developed at ONERA [29]. It is able to handle TS and traveling crossflow instabilities.

2. *DLR's Tool*

For the tool used by DLR, the chosen strategy is the coupling of a RANS solver with two e^N methods, one for TS instabilities and one for crossflow instabilities, through a boundary-layer code based on the local 2.5-D approach. Details of the two e^N methods used can be found in [25]. The general strategy retained for the DLR's tool is illustrated in Fig. 10.

The solver used by DLR for RANS computation is the FLOWer code. It is a three-dimensional compressible RANS code for steady

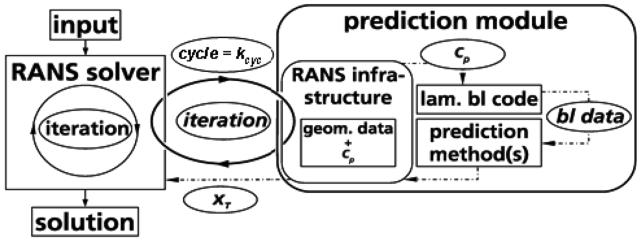

Fig. 10 General strategy used for transition prediction in DLR's tool (bl denotes the boundary layer).

or unsteady flow problems and uses structured body-fitted multiblock meshes. The code is based on a finite volume formulation and provides a cell vertex as well as a cell-centered spatial discretization scheme using central differencing. Dissipative terms are explicitly added to damp high-frequency oscillations and to achieve a sufficiently sharp resolution of shock waves. The dissipative operator comprises second-order k_2 and fourth-order k_4 differences scaled by the largest eigenvalue, as in Jameson-like numerical schemes. The time integration is carried out using an explicit hybrid multistage Runge–Kutta scheme. For steady-state calculations, the integration is accelerated by local time stepping and implicit residual smoothing. These techniques are embedded in a multigrid algorithm. The influence of turbulence is taken into account either by eddy viscosity turbulence models according to the Boussinesq approximation or by algebraic or differential Reynolds stress models. The transition handling is independent of the block topology of the computational grid and of the grid structure (structured, unstructured, or hybrid grid) [30]. The transition-prediction module coupled to the FLOWer code consists of a laminar boundary-layer method for swept tapered wings and several transition-prediction methods, which are provided with all necessary boundary-layer data by the laminar boundary-layer method.

The laminar boundary-layer method solves the compressible laminar boundary-layer equations for conical external flow. In addition to a number of empirical transition criteria, the most general transition-prediction methods that are currently available are an e^N database method for TS instabilities and an e^N database method for crossflow instabilities.

The application of a boundary-layer method for the computation of all viscous data necessary for the transition-prediction method ensures the high accuracy of the viscous data required by the e^N methods for the analysis of laminar boundary layers. Thus, the large number of grid points near the wall for a high resolution of the boundary layers; the adaptation of the Navier–Stokes grid in the laminar, turbulent, and transitional boundary-layer regions; and the generation of new adapted grids for the RANS solver after every step of the transition location iteration are avoided and the computational time can be massively reduced. In addition, the number of RANS iteration cycles between two steps of the transition location iteration can be highly reduced compared with an approach in which the boundary-layer parameters are computed directly from the RANS grid, because the surface pressure converges significantly faster in the RANS computation than the boundary-layer velocity profiles that are the basis for the computation of the boundary-layer parameters.

3. *ONERA's Tool*

For the tool used by ONERA, the chosen strategy is the coupling of a RANS solver with application of transition criteria using the boundary-layer characteristics directly issued from the RANS solution. The general strategy retained for ONERA's tool is illustrated in Fig. 11.

The solver used by ONERA for RANS computation is the elsA software, which solves the compressible three-dimensional RANS equations by using a cell-centered finite volume spatial discretization on structured multiblock meshes. Computations are carried out using an uncoupled approach between the RANS system and the turbulence model transport equations. For the explicit scheme, a 4-

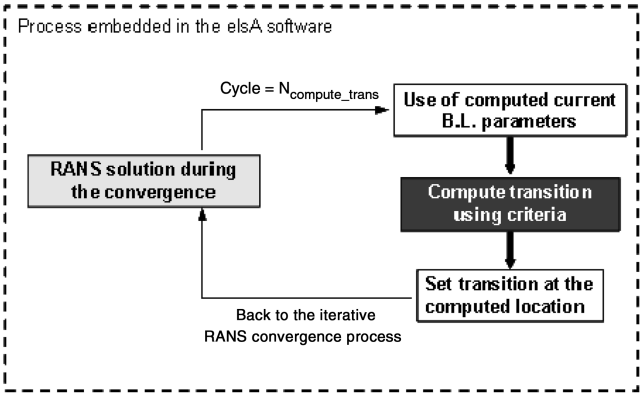

Fig. 11 General strategy used for transition prediction in ONERA's tool.

step Runge–Kutta space-centered Jameson-like scheme, is used for the conservative variables. A fourth-order linear dissipation is generally used (k_4), with added second-order dissipation terms k_2 for treatment of flow discontinuities. For the implicit stage, a lower/upper symmetric successive over-relaxation numerical scheme is associated with an Euler backward time integration scheme, which allows fast convergence rates on classical configurations. For the turbulent variables, the Roe numerical scheme is used. Different multigrid techniques are available for convergence acceleration (V or W cycles) as well as for low-speed preconditioning. A number of turbulent models are available (Spalart–Allmaras, k-ω, k-l, differential Reynolds stress model, etc.) with wall treatment based on damping functions or wall laws.

Transition-prediction capability has been introduced into the elsA code [4], based on application of criteria that were developed at ONERA for use in boundary-layer codes, such as bypass, TS and crossflow transition, and laminar-separation-bubble predictions. those considered relevant here are, namely, the Arnal–Habiballah–Delcourt criterion for TS instabilities, the C1 criterion for crossflow instabilities, and the Gleyzes–Habiballah criterion for 2-D short bubble transition. These criteria, described in Sec. II, are functions of the incompressible shape factor of an averaged Pohlhausen parameter Λ_2 of the crossflow displacement integral length δ_2 and of the external turbulence level T_u. Integral lengths are directly computed from the velocity field, but the shape factor is obtained indirectly as a function of the Pohlhausen parameter. Therefore, standard grid resolutions can be used. In the laminar part of the flow, the intermittency function Γ is set to zero, then turbulence starts, usually some distance downstream of the detected transition location. The laminar flow region extends in the direction normal to the wall up to about 1.3 times the boundary-layer thickness to ensure a natural flow physics for wake developments and to avoid problems pointed out in Sec. III.B. Up to now, the intermittency function used is a step function in its simplest form. Use of more sophisticated intermittency functions is being explored at ONERA.

There is no prediction of attachment-line contamination in the current exploitation version of elsA used for these computations or of relaminarization. These parts have been added at the end of the EUROLIFT II project and were validated on specific test cases. They have not been validated yet in a high-lift context.

4. *Other Partners' Tools*

In EUROLIFT II, two partners, CIRA and FOI, carried out computations with transition prescribed. The main characteristics of the CFD solvers used are given next.

For CIRA, the RANS solver used is the structured multiblock finite volume code ZEN. In the current computations, a cell-centered scheme was used for spatial discretization and stability was ensured by applying a Jameson-like artificial dissipation scheme. In particular, the second-order dissipation coefficient was set to zero due to the low freestream Mach number. The explicit 3-stage Runge–Kutta scheme was used for the pseudotime integration, whereas the use of both implicit residual averaging and a multigrid technique enabled faster convergence rates to be achieved. The turbulence model considered is the turbulent/nonturbulent version of the Kok k-ω model.

For FOI, the RANS code used is the unstructured EDGE solver, based on a finite volume approach with dual grids. The solver adopts an edge-based formulation for arbitrary elements and uses a node-based finite volume technique to solve the governing equations. Two spatial discretizations of convection are available in combination with a compact discretization of the viscous terms. The governing equations are integrated explicitly toward steady state with Runge–Kutta integration. The convergence is accelerated with agglomeration multigrid and implicit residual smoothing. The turbulence model considered is a k-ω explicit algebraic Reynolds stress model.

IV. Configurations Considered

The two high-lift configurations considered in this paper are presented in Fig. 12 and are briefly described hereafter.

A. AFV Model

The AFV model is a multi-element constant-chord swept wing based on a RA16C profile with a reference chord of 0.5 m (in the normal to leading-edge direction). The wing span is 2 m from tunnel floor to tip when the sweep angle is 40 deg. Pressure rows, slat and flap tracks fairing, and wing tip are parallel to the floor for this sweep angle. This model was tested in the pressurized ONERA F1 wind tunnel during the EUROLIFT I project at a constant Mach number $M_0 = 0.2$, with varying Reynolds number (Re_C from 2.8×10^6 to 9×10^6), two values of sweep angle (30 and 40 deg), and two values of flap deflection (20 and 40 deg). The model is equipped with 8 rows of 93 pressure taps (a total of 744) distributed over the 3 elements. The experiments were especially designed for the study of laminar-turbulent transition [26], which was detected using 24 wall hot films and infrared thermography, in addition to the more usual force and wall pressure measurements. The experimental conditions were such that the main wing element is almost always contaminated, and transition may be observed on the slat and the flap.

Hence, this model allows the observation of all the phenomena under discussion: natural transition, attachment-line contamination, laminar bubble separation, and relaminarization. Full relaminarization was not observed, but instead, a characteristic reduction in fluctuations that could be associated to flow acceleration. The experimental database obtained on this model is used for validation of numerical methods (simple configuration).

All the results presented in this paper are obtained for the flow condition $M_0 = 0.20$ and $Re_C = 2.8 \times 10^6$ for the reference configuration of a sweep angle of 40 deg and flap deflection of 20 deg.

B. KH3Y Model

The KH3Y model is a half-plane model equipped with a modern-type wing designed by Airbus Germany in the course of a German national research project. It was selected for use in the EUROLIFT I

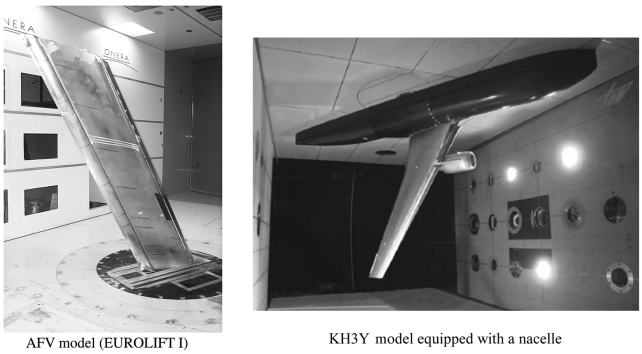

AFV model (EUROLIFT I) KH3Y model equipped with a nacelle

Fig. 12 Three-dimensional high-lift configurations considered in the EUROLIFT projects.

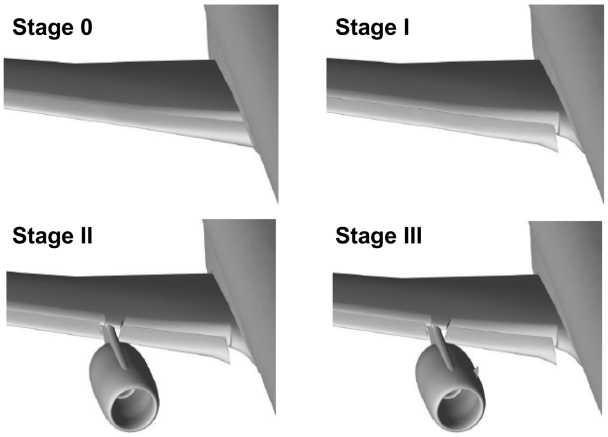

Fig. 13 Complexity levels of the KH3Y high-lift model considered in the EUROLIFT projects.

and II projects for tests in a number of configurations, from clean wing to advanced flap system with pylon and nacelle (Fig. 13), both in the Airbus Germany low-speed wind-tunnel (LSWT) facility and in the pressurized cryogenic ETW wind tunnel.

The first series of tests at the low-speed wind tunnel were realized with a three-element full-span slat and flap wing without nacelle, in both takeoff and landing configurations, at a single chord Reynolds number of 1.38×10^6 and at Mach 0.178. A second series of test at ETW were carried out later, up to high Reynolds numbers ($Re_C = 25 \times 10^6$) [31].

The landing configuration with slat and flap settings of 26 and 32 deg, respectively, was selected for transition work because a larger set of transition observations was available in that configuration. The model was equipped with several arrays of hot films placed on the carbon fiber slat and on the main wing leading-edge region and was observed using two infrared cameras. Analysis focused on the slat and wing hot films located at midspan of the outer wing.

All the results presented in this paper are for the flow condition $M_0 = 0.178$ and $Re_C = 1.35 \times 10^6$ for the stage-0 configuration.

V. Numerical Results

A. Transition Prescribed

A first set of computations has been carried out by CIRA on the KH3Y takeoff configuration and by FOI, ONERA, and DLR on the KH3Y landing configuration, by considering transition fixed at a given location on the different elements, derived from the experiments (level 1 for the transition model).

For the takeoff case, CIRA used experimental transition locations available at only one outboard-wing section (DV7) and for $\alpha = 12$ and 16 deg. Such locations were extrapolated both in the spanwise direction ($x_{tr}/c = \text{const}$ assumed) and in the α range for prescribing the transition locations close to the stall conditions. The results show an increase in lift coefficient, which improves the correlation with experimental data in the linear part of the $C_L(\alpha)$ curve (Fig. 14). This is well explained by the improved prediction of the expansion peaks at both the slat and main wing leading edges shown in the pressure distributions. However, there is no improvement observed for the $C_{L\max}$ estimation. Possible explanations are the aforementioned extrapolations as well as the more robust numerical settings required for the prescribed transition computations. Furthermore, it must be noted that geometrical details (such as slat or flap track fairing), not considered in the current computations, significantly affect the maxim lift of the KH3Y configuration.

At the measuring wing section DV7, the hot-wire measurements revealed the existence of a laminar separation followed by transition and turbulent reattachment at the slat leading edge (i.e., a laminar separation bubble). The transition line specified in computations was therefore located between the experimental separation and the reattachment points, according to the indicated hot-wire transition location. It is very interesting to note that the (laminar) separation line obtained by CFD is very close to the measured one, as depicted in Fig. 15.

However, due to the mentioned spanwise extrapolation, when looking at the inboard wing, a quite important separation bubble is computed that was not observed during experiments. In this area, the prescribed transition line is probably located too far downstream compared with its real location. Based on the findings of the study of laminar separation bubbles carried out by FOI and presented in Sec. II.D, prescribing a transition line too far downstream leads to an overestimation of the boundary-layer thickness and of the size of the separation bubble.

The same behavior has been observed with the solvers from the different partners on the landing configuration, whatever the grid technique used (structured or unstructured) or the turbulence model. As an illustration, Fig. 16 presents the friction lines obtained by FOI on the landing configuration, where a separation bubble is computed on the slat at inboard and outboard span locations.

The problem is that it is very difficult to know whether the solution obtained is correct or not. As was noted previously, the impact of transition on C_p distribution is very small, and the solution looks realistic. For instance, for the FOI results considered here, pressure distribution at a midspan wing section matches well with experimental data. Therefore, it is necessary to consider complex transition lines during the convergence of the flow solution and to frequently adapt these transition lines during the convergence iterative process. In the first part, the ONERA and INTA tools were validated on the AFV configuration. For the more realistic KH3Y landing case, the DLR and ONERA tools were used.

B. Transition Internally Computed: Validation on the AFV Configuration

The method of nonlocal transition implemented in the ONERA elsA software, as well as the 2.5-D tool developed at INTA, was

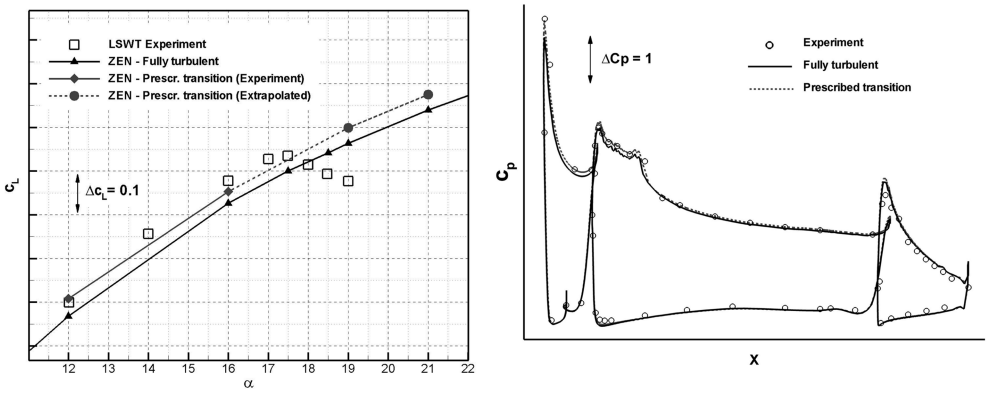

$C_L(\alpha)$ curve M=0.178 , Re= 1.35×10^6 Pressure distribution at midboard wing for α=12 deg

Fig. 14 KH3Y model, takeoff configuration; CIRA results with transition prescribed.

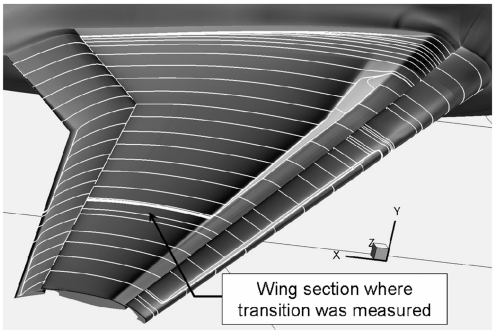

Computed friction lines on the complete wing

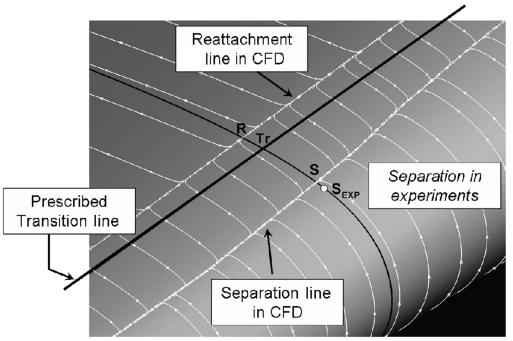

Computed friction lines at measuring wing section.

Fig. 15 CIRA computations ($\alpha = 12$ deg); friction lines with transition prescribed in the computations.

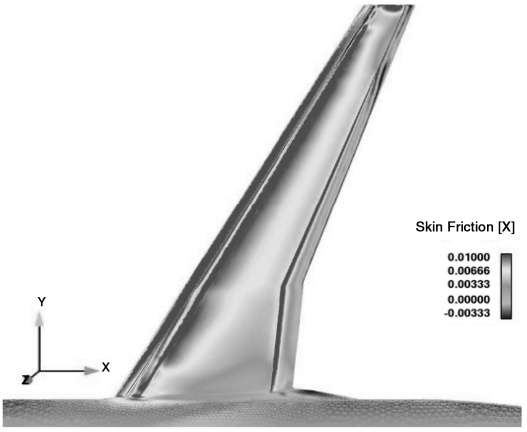

Separation bubble found on the inboard and outboard slat

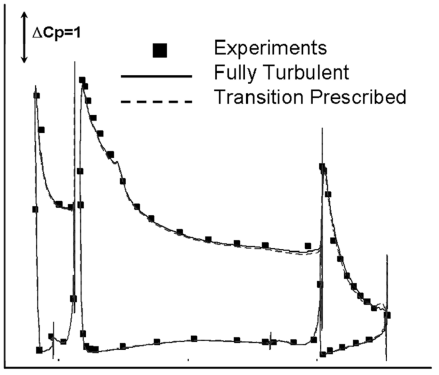

Pressure distribution at midboard wing (α=12 deg)

Fig. 16 KH3Y model in landing configuration; results of FOI computations with transition prescribed.

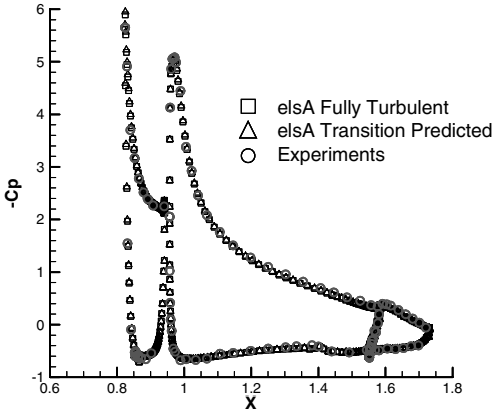

Comparison between experiment, elsA in fully turbulent mode and with transition criteria

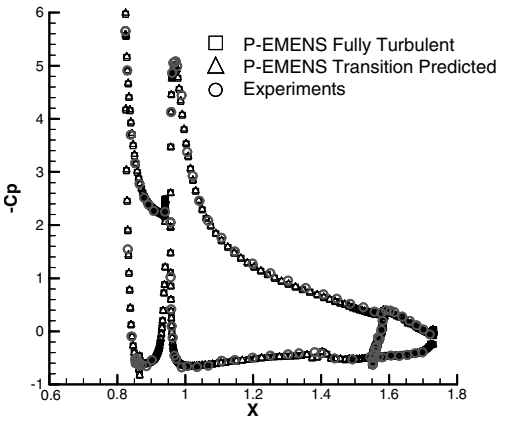

Comparison between experiment, P-EMENS in fully turbulent mode and INTA's transition prediction tool

Fig. 17 AFV model: comparison of C_p distributions at $Y/B = 55.2\%$ for $\alpha = 22.5$ deg.

validated on the AFV wing. The RANS flow computations of the 3-element AFV model are performed in 3-D, assuming that the model is placed in a semi-infinite space with a symmetry condition at the wing root. It was verified that both RANS solvers perform well in this case and produce good prediction of surface pressures, which is necessary for correct transition prediction. It was also found that in the linear zone, taking into account transition had no impact on the pressure distributions (Fig. 17), as confirmed by the experimental results for the range of Reynolds numbers considered. Leading-edge contamination on the main element was clearly predicted and both methods gave coherent results for the location and type of natural transition on the upper side of the slat, in good agreement with measurements.

Figure 18 compares the evolution of the transition line on the slat when the angle of attack increases for both codes. The same global behavior is obtained for both methods, either considering a coupling with a 2.5-D boundary-layer code or by the use of criteria internally computed. In addition, the three-dimensionality of the transition line can clearly be seen in this figure, particularly for $\alpha = 15$ and 17.5 deg.

Finally, no influence of transition prediction on lift and drag was found in the linear zone of the polar plot, as it could be deduced from pressure distributions; nevertheless, a visible impact was shown close to maximum lift (Fig. 19). The limited effect of transition on drag coefficient can be explained when considering the very limited contribution of friction drag to the total drag: the pressure component

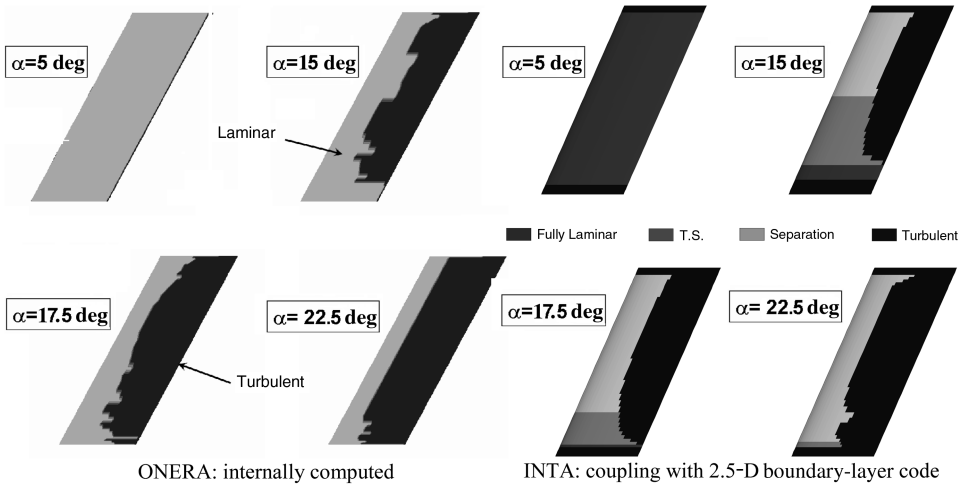

Fig. 18 AFV model: transition location computed on the slat upper surface by ONERA or INTA tools.

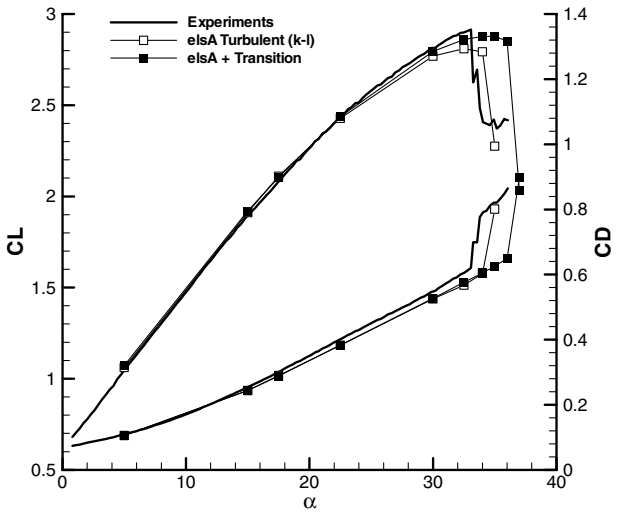

Fig. 19 AFV model: effect of transition taken into account in the computations; comparison of ONERA results with experiments.

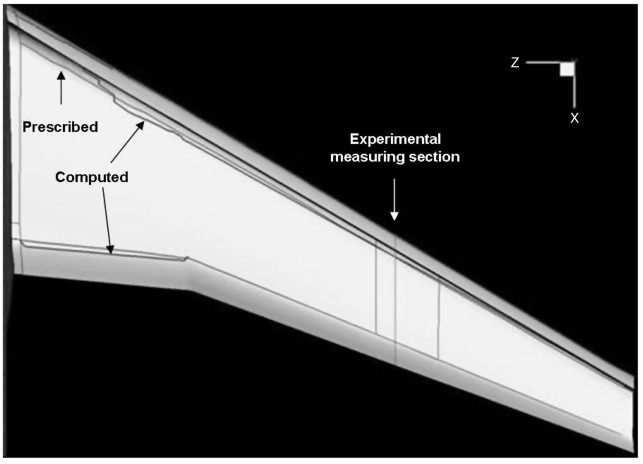

Fig. 20 KH3Y model in landing configuration; comparison between computed and prescribed transition areas ($\alpha = 14$ deg); DLR computations.

is preponderant. In addition, the outcomes of far-field drag analysis carried out in EUROLIFT II on the KH3Y configuration have shown that for a high-lift configuration, lift-induced drag is the preponderant contribution to the total drag coefficient (from 50 to 80%, depending on C_L). Therefore, an accurate estimation of drag is directly linked to an accurate estimation of pressure field and therefore of lift.

C. Effect of Transition on the Performance of a Realistic High-Lift Configuration

In the EUROLIFT II project, computations on the KH3Y landing configuration considering transition internally predicted in the CFD solvers were carried out by ONERA and DLR on a limited number of angles of attack, as this exercise was a pioneering one for such a case. Note that the main differences between these two methods are the transition-prediction tool itself (local 2.5-D database methods for DLR, combination of criteria for ONERA) and the way transition lines are computed (some grid sections and between interpolations for DLR and based on the surface grid for ONERA). Figure 20 compares the transition lines computed by DLR on the KH3Y case in a landing configuration for $\alpha = 14$ deg with the prescribed zones. It can be seen that the different areas are comparable, but some differences are noticeable, especially in the inboard main wing. In this region, the extrapolation of transition lines from the outboard sections, where some instrumentation were available, leads to an overprediction of the extension of laminar flow. Differences observed seem small but, as a consequence, the flow physics compatibility is always ensured during the computations, and for some sections, the separated areas observed when transition is prescribed disappears when transition is computed (see, for instance, wing section 4 in Fig. 21).

For the computations carried out by ONERA on the same configuration, similar findings have been observed and Fig. 22 compares the evolution of laminar area extents between $\alpha = 10$ and 12 deg on the different elements. The decrease of laminar area on the slat upper surface due to the change of pressure gradient at the leading edge is visible. Here again, taking the three-dimensionality of the transition line during the computations significantly improves the agreement with experimental pressure distributions, particularly for the outboard sections (Fig. 23).

For the flap upper surface and the main wing lower surface, the modifications are quite limited, as the pressure distributions on these sides do not change a lot for these conditions.

It should be noted that at the present time, it is not possible to know which phenomenon triggers transition in elsA (TS, bubbles, or crossflow), but this functionality will be available in future versions. However, in the framework of EUROLIFT II, ONERA has developed an interface between a RANS solution and a 3-D boundary-layer code using the 3-D transition-prediction method. This interface has been used on the turbulent solution, which is slightly different from the transitional one. However, when considering surfaces for which the pressure field is nearly identical in both cases, and with a significant laminar flow extent, such as the

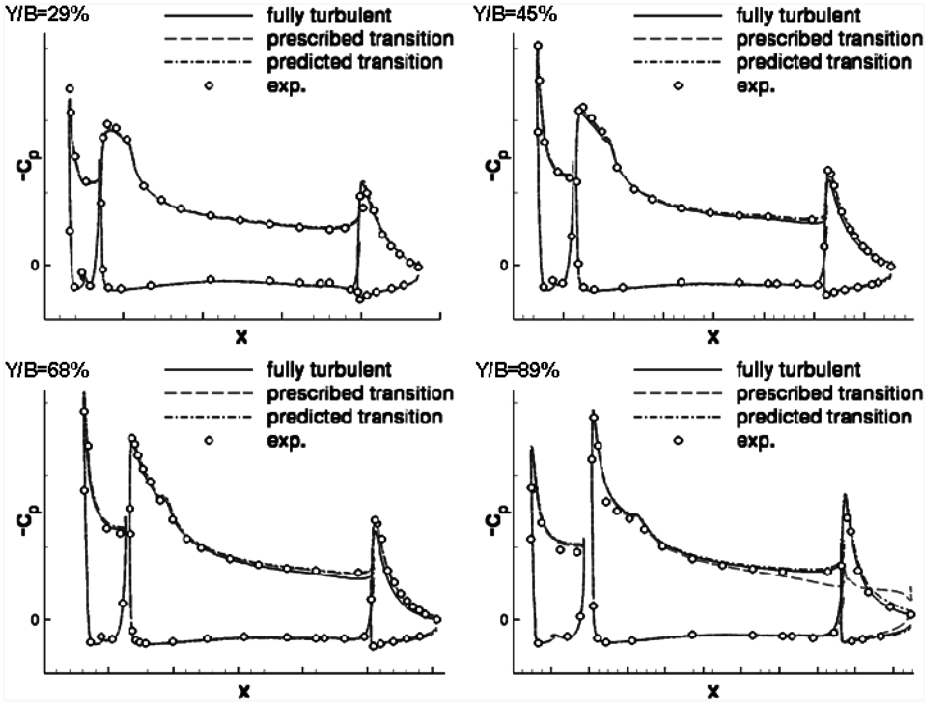

Fig. 21 KH3Y model in landing configuration ($\alpha = 14$ deg); comparison of computed C_p distribution with measurements; DLR results.

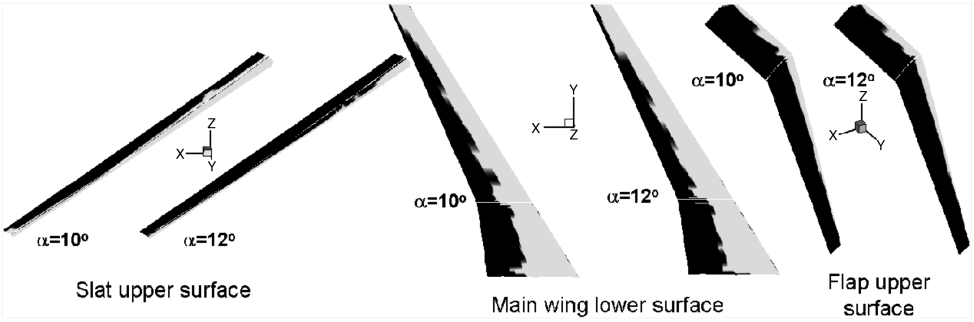

Fig. 22 KH3Y model in landing configuration; evolution of computed transition lines with the ONERA tool between $\alpha = 10$ and 12 deg.

main wing lower surface, it can be noted that the laminar areas issued from computations with transition internally computed are comparable with the transitional areas computed by boundary-layer code on the turbulent solution (Fig. 24).

A practical solution could be to compute the pressure field taking transition into account during the iterative process, to have the impact on performance simulated, and then to carry out the analysis using 3-D boundary-layer code but on the transitional pressure field. However, the most important phenomenon to model is the impact of transition on performance. Therefore, transition tools have to produce a realistic transition line location so that change in performance could be estimated by CFD solvers. The nature of transition process comes in a second step.

Finally, ONERA carried out computations at high angles of attack to check whether or not transition could affect the numerical estimation of maximum lift compared with turbulent computations; results are presented in Fig. 25. Numerically speaking, maximum lift occurs at a lower angle of attack (2 deg below) than for turbulent cases. As observed previously on other configurations, there are no visible effects of transition for angles of attack below maximum lift, and numerical predictions compare quite well with the measurements. There is still an overestimation of $C_{L\max}$ by computations, compared with experimental data. However, a significant effect of geometrical details on $C_{L\max}$ has been demonstrated for this configuration (in particular, the slat and flap track fairings, which were not considered in the current case). Also, wing deformation, tunnel setup, peniche, and tunnel walls all have an impact on force coefficients at high angles of attack. Therefore, the final step for an accurate estimation of the performance of this landing configuration has to consider transition-prediction tools and geometrical details at the same time.

D. Effect of Reynolds Number on Performance on a Clean-Wing Configuration

The final study dealing with transition carried out in EUROLIFT II was the investigation of the effect of the Reynolds number on the performance of a clean-wing configuration at low speed. The KH3Y clean-wing case, equipped with a standard or a modified leading edge (a drooped nose), was investigated in the EUROLIFT I project and some significant evolutions of $C_{L\max}$ were found from the ETW results between $Re = 1.65 \times 10^6$ (ambient conditions) and $Re = 9 \times 10^6$ (pressurized cryogenic condition). At that time, the measurements considered force and pressure on the wing only, and it was assumed that this evolution of $C_{L\max}$ with Reynolds number could be due to transition changes on the wing, which was not measured. Therefore, it was proposed to use the partners' numerical capabilities to take transition into account in their solver in the current code version and to investigate 1) if transition moves significantly and 2) if it affects the maximum lift. ONERA carried out this exercise, whereas FOI carried out the Reynolds number effect on a fully turbulent case. Results obtained by FOI were very similar to

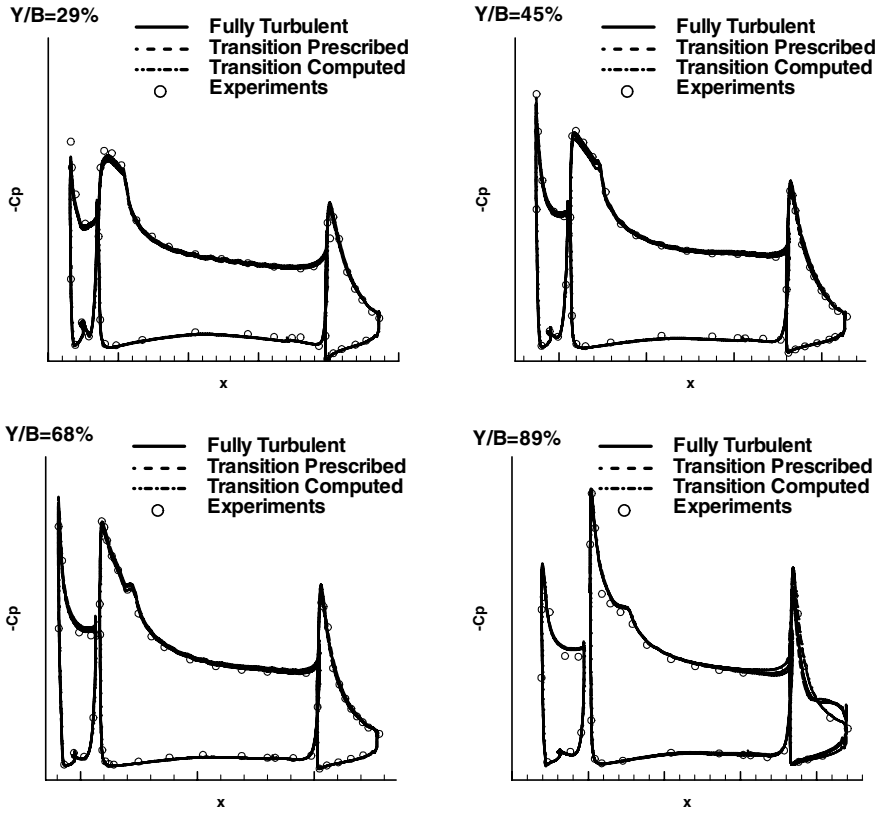

Fig. 23 KH3Y model in landing configuration ($\alpha = 12\,\mathrm{deg}$); comparison of computed C_p distribution with measurements; ONERA results.

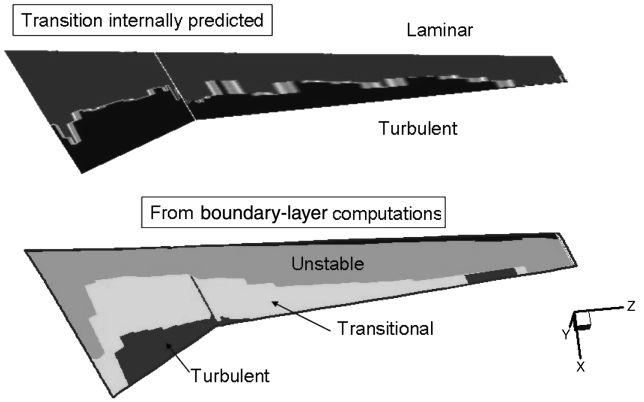

Fig. 24 KH3Y model in landing configuration ($\alpha = 10\,\mathrm{deg}$); comparison of the boundary-layer state between RANS and criteria computations and 3-D boundary-layer code on the main wing lower (ONERA results).

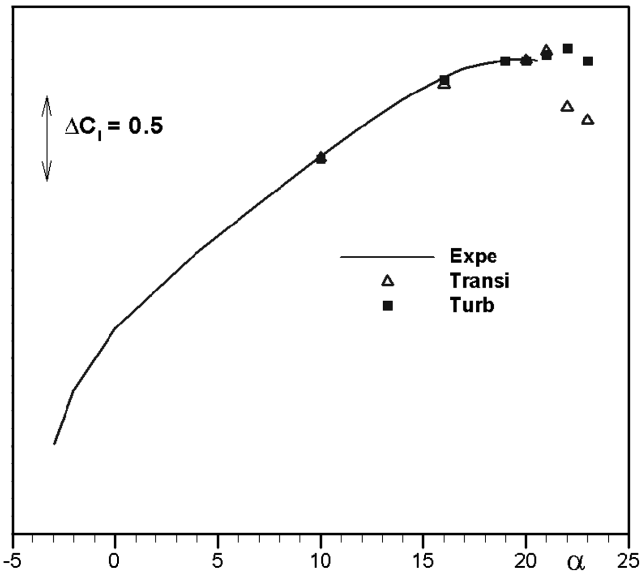

Fig. 25 KH3Y model in landing configuration; comparison of computed $C_L(\alpha)$ curves with experiments (ONERA results).

the fully turbulent results obtained by ONERA; therefore, only the ONERA results are presented here for consistency of the comparison with transitional cases. Figure 26 presents the surface mesh generated by ONERA. Some details of the standard and modified lead-edge shapes are also presented.

Figures 27 and 28 compare the computed $C_L(\alpha)$ curves with the measured ones for the standard leading edge and the drooped nose, respectively, for low and high Reynolds conditions. Vertical bars represent the amplitude of oscillations in the convergence curve. Of course, some discrepancies with experimental data remain, but the following points have been observed:

1) In the linear part of the $C_L(\alpha)$ curve, both lift coefficients and C_p distribution on the wing compare well with experiments. Taking transition into account at a constant angle of attack leads to a better agreement at that point.

2) Taking the transition into account leads to a significant improvement of the evaluation of maximum lift ($C_{L\max}$) and $\alpha(C_{L\max})$, compared with turbulent results. In addition, it was observed that the effect of transition on maximum-lift evaluation is different between the low Reynolds number case ($Re = 1.65 \times 10^6$) and the high Reynolds number case ($Re = 9 \times 10^6$):

a) For $Re = 1.65 \times 10^6$, $C_{L\max}$ decreases when transition is taken into account; this implies that maximum lift at this Reynolds number is significantly dependent on the boundary-layer characteristics on the wing. For the drooped-nose configuration, there is an overestimation of $C_{L\max}$, probably due to laminar separation bubbles not well simulated.

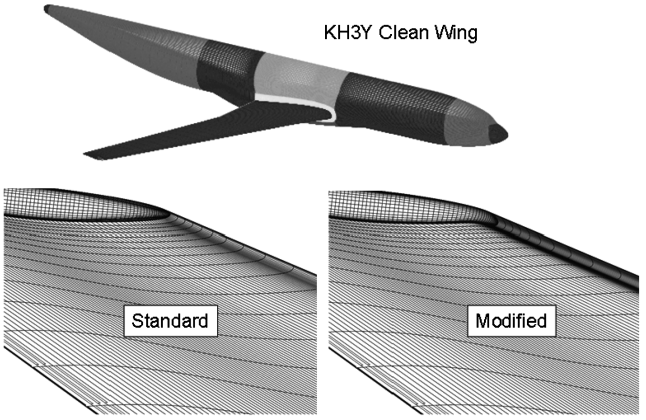

Fig. 26 KH3Y model, clean-wing configuration; surface grid and detail of the standard and modified leading-edge shapes.

b) For $Re = 9 \times 10^6$, $C_{L\max}$ slightly (for standard leading edge) or significantly (for drooped nose) increases when transition is taken into account, but not $\alpha(C_{L\max})$. This implies that transition has an effect on the absolute level of lift but does not change the physical phenomenon that drives maximum lift. This is particularly visible on the results on the drooped-nose configurations.

3) The experimental evolution of C_p on the outboard wing at constant angle of attack when Reynolds number increases is simulated by CFD only if transition is taken into account. Turbulent computations lead to a similar pressure field for both $Re_C = 1.65 \times 10^6$ and 9×10^6 (Fig. 29).

Finally, the estimation of the evolution of $C_{L\max}$ with the Reynolds number is significantly improved by computations with transition taken into account, compared with turbulent results, as can be seen in Fig. 30. Of course, some differences remain, but some important features such as the model deformation or geometrical details (the flap track fairings were still present, although the configuration was not a high-lift one) were not taken into account in the present

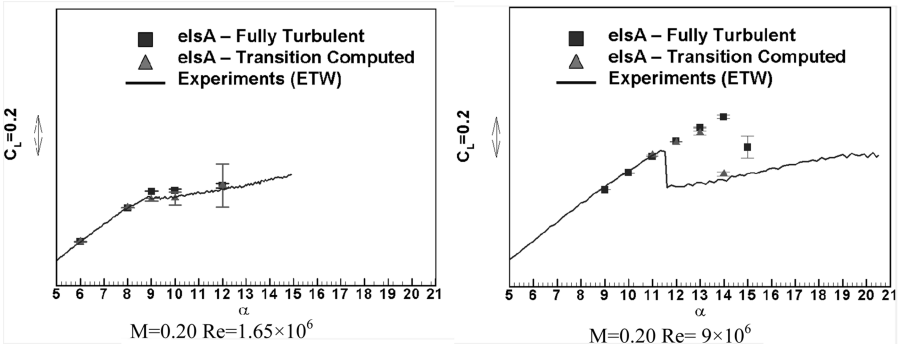

Fig. 27 KH3Y clean configuration, standard leading edge; effect of transition on computed $C_L(\alpha)$ curves at $Re = 1.65 \times 10^6$ and 9×10^6; comparison with experiments.

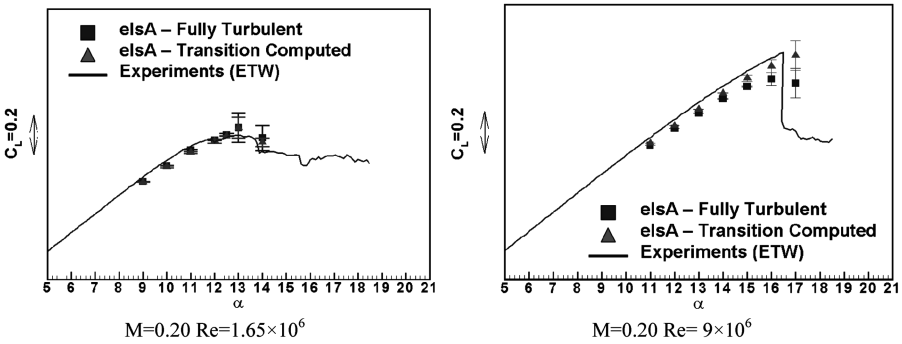

Fig. 28 KH3Y clean configuration, modified leading edge; effect of transition on computed $C_L(\alpha)$ curves at $Re = 1.65 \times 10^6$ and 9×10^6; comparison with experiments.

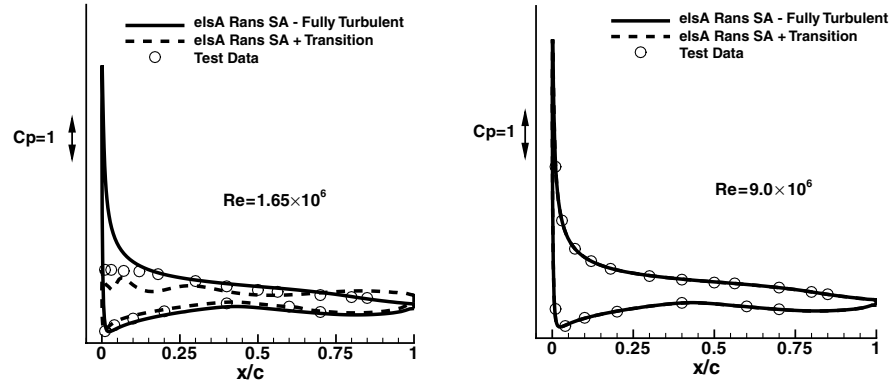

Clean wing configuration – M=0.20 – α=9° – pressure distribution at y/b= 89%

Fig. 29 KH3Y clean-wing configuration, standard leading edge; effect of Reynolds number on pressure distribution at an outboard-wing section; comparison between computations (turbulent and transitional) and experiments.

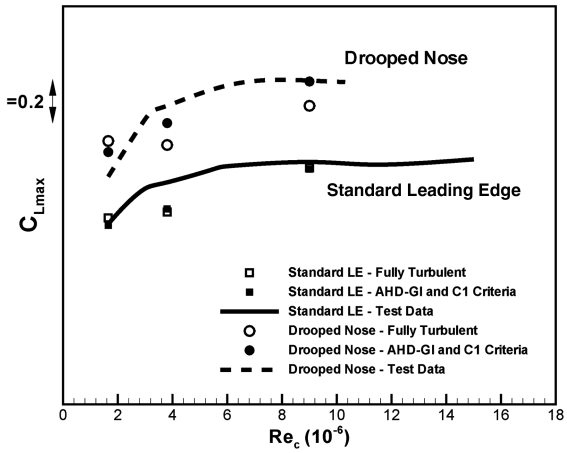

Fig. 30 KH3Y clean-wing configuration; evolution of maximum lift with Reynolds number; comparison of CFD results with experiments (LE denotes the leading edge).

computations. Therefore, it can be stated that most of the evolution of maximum lift observed can be attributed to an effect of transition.

VI. Conclusions

For an accurate estimation of the aerodynamic performance of an aircraft in high-lift configuration, transition from laminar to turbulent flow must be considered either for the analysis of a subscale wind-tunnel test campaign, to extrapolate the performance to flight conditions, or in the full-scale computations used for prediction. Thanks to the research projects EUROLIFT and EUROLIFT II, a better knowledge of the role played by transition on the performance of high-lift configurations has been reached on both the experimental side through the use of the ETW cryogenic wind tunnel and on the numerical side through the introduction of automatic transition-prediction tools in different RANS solvers.

In the first part, it was verified that computations with transition prescribed using experimental results at limited wing sections led to an improvement of the performance prediction, but close to maximum lift, the complex shape of the transition line on the wing surface must be considered to produce a more realistic solution. In particular, when separation bubbles are present, a high sensitivity of the bubble size to the prescribed transition location has been shown.

Then three different tools considering transition-prediction codes coupled with a RANS solver were evaluated on different configurations. Two of them considered a transition prediction based on boundary-layer code under the local 2.5-D assumption. However, extension to real 3-D flow seems possible in the near future, under the condition that a proper interface tool is available. In addition, it should be noted that boundary-layer tools cannot compute separated flows, which are often present on a high-lift configuration, which may be a practical limitation for such tools.

The third method considered uses transition criteria based on the boundary-layer characteristics directly issued form the RANS solution. To overcome the problem of accuracy for boundary-layer evaluation due to the generally insufficient grid density of standard meshes in the boundary layer, formulations are based on the Pohlhausen parameter instead of the velocity profiles. However, in that case, a sufficient grid resolution in the streamwise direction is required.

A first validation work based on clean-wing configurations at low speed have shown that the effect of the change in Reynolds number is well captured by the numerical simulation when taking transition into account. It was also observed that the effect of transition on $C_{L\max}$ is a Reynolds-dependent phenomenon: a decrease of $C_{L\max}$ is computed for low Reynolds numbers, whereas an increase of $C_{L\max}$ is computed for high Reynolds numbers, compared with turbulent cases.

Results obtained by these different tools are quite comparable, and further evaluations are necessary to check if one of the strategies proves better than the other. However, it should be noted that some developments are still ongoing for these tools. For instance, the introduction of leading-edge contamination and relaminarization criteria in the ONERA tool and the introduction of stability calculations in the DLR code are underway, with validation foreseen in the near future. However, the mandatory capability of such a tool is not only to compute the exact location and nature of transition (TS, crossflow, bubbles, etc.) at given wing sections, but to be able to deal with a complex 3-D transition line, so that the impact on performance can be evaluated by CFD solvers.

Finally, based on the outcomes from other work packages in EUROLIFT II, future validation work will have to take these different parameters into account all together: 1) transition (in particular, for separation bubbles), 2) geometrical details (such as flap track fairing), 3) model deformations, and 4) tunnel setup (walls and peniche).

Acknowledgments

The research work discussed in the paper was performed under the European research contract G4RD-CT-1999-00072 in the EUROLIFT project as part of the fifth framework program and under contract AST2-2004-502896 in the EUROLIFT II project as part of the sixth framework program, which were cofinanced by the European Commission. The authors also thank all the involved EUROLIFT partners, especially Gery Vidjaja (Airbus-Deutschland) and Philippe Bardoux (ONERA), who produced the structured meshes for the KH3Y configurations.

References

[1] Haines, A. B., *Scale Effects on Aircraft and Weapon Aerodynamics*, edited by A. D. Young, AGARDograph AG-323, AGARD, Neuilly-sur-Seine, France, July 1994, pp. 27–66.

[2] Lindblad, I., and de Cock, K., "CFD Prediction of Maximum Lift of a 2-D High-Lift Configuration," 17th AIAA Applied Aerodynamics Conference, AIAA Paper 99-3180, Norfolk, VA, June 1999.

[3] Moens, F., "Garteur AD-AG25: CFD Prediction of Maximum Lift of a 2-D High-Lift Configuration," *KATnet/GARTEUR High-Lift Workshop*, edited by J. Fulker, Stockholm, Sweden, Sept. 2002.

[4] Moens, F., Perraud, J., Séraudie, A., and Houdeville, R., "Transition Measurement and Prediction on a Generic High-Lift Swept Wing," *Proceedings of the Institution of Mechanical Engineers, Part G (Journal of Aerospace Engineering)*, Vol. 220 June 2006, pp. 589–603. doi:10.1243/09544100JAERO85

[5] Toulorge, T., Ponsin, J., Perraud, J., and Moens, F., "Automatic Transition Prediction for RANS Computations Applied to a Generic High-Lift Wing," 45th AIAA Aerospace Sciences Meeting and Exhibits, AIAA Paper 2007-1086, Reno, NV, Jan. 2007.

[6] Krumbein, A., "Automatic Transition Prediction and Application to 3-D High-Lift Configurations," 24th AIAA Applied Aerodynamics Conference, San Francisco, AIAA Paper 2006-3164, June 2006.

[7] Pfenninger, W., "Flow Phenomena at the Leading Edge of Swept Wing," *Recent Developments in Boundary Layer Research*, Pt. 4, AGARDograph AG-97, AGARD, Neuilly-sur-Seine, France, May 1965.

[8] Poll, D. I. A., "Some Aspects of the Flow Near a Swept Attachment Line with Particular Reference to Boundary Layer Transition," College of Aeronautics TR 7805, Cranfield, England, U.K., Aug. 1978.

[9] Beasley, A., "Calculation of the Laminar Boundary Layer and Prediction of Transition on a Sheared Wing," Royal Aeronautical Establishment, TR 3787, Farnborough, England, U.K., Oct. 1973.

[10] Arnal, D., and Juillen, J. C., "Leading Edge Contamination and Relaminarization on a Swept Wing at Incidence," *Numerical and Physical Aspects of Aerodynamic Flows 4*, edited by T. Cebeci, Springer–Verlag, New York, 1990, pp. 391–402.

[11] Arnal, D., "Three-Dimensional Boundary Layers: Laminar-Turbulent Transition," *Computations of Three-Dimensional Boundary Layers Including Separation*, AGARD Rept. 741, AGARD, Neuilly-sur-Seine, France, 1986.

[12] Arnal, D., "Transition Prediction in Transonic Flow," *IUTAM Symposium Transsonicum 3*, Springer–Verlag, Berlin, 1989, pp. 253–262.

[13] Casalis, G., and Arnal, D., "ELFIN II Subtask 2.3: Data Base Method Development and Validation of the Simplified Method for Pure Crossflow Instability at Low Speed," ONERA TR 145, Toulouse, France, Dec. 1996.

[14] Gregory, N., Stuart, J. T., and Walker, W. S., "On the Stability of Three Dimensional Boundary Layer with Application to the Flow due to a Rotating Disc," *Philosophical Transactions of the Royal Society of London, Series A: Mathematical and Physical Sciences*, Vol. 248, No 943, 1955, pp. 155–199. doi:10.1098/rsta.1955.0013

[15] Gaster, M., "A Note on the Relation Between Temporally Increasing and Spatially Increasing Disturbances in Hydrodynamic Stability," *Journal of Fluid Mechanics*, Vol. 14, 1962, pp. 222–224. doi:10.1017/S0022112062001184

[16] Gleyzes, C., Cousteix, J., and Bonnet, J. L., "Theoretical and Experimental Study of Low Reynolds Number Transitional Separation Bubbles," *Proceedings of the Conference on Low Reynolds Number Airfoil Aerodynamics*, edited by Th. J. Mueller, Univ. of Notre Dame Notre Dame, IN, June 1985, pp. 137–152.

[17] Cliquet, J., Houdeville, R., and Arnal, D., "Application of Laminar-Turbulent Transition Criteria in Navier–Stokes Computations," 45th AIAA Aerospace Sciences Meeting and Exhibits, Reno, NV, AIAA Paper 2007-515, Jan. 2007.

[18] Perraud, J., and Moens, F., "Transport Aircraft 3-D High-Lift Wing Numerical Transition Prediction," 45th AIAA Aerospace Sciences Meeting and Exhibits, Reno, NV, AIAA Paper 2007-264, Jan. 2007.

[19] Wilcox, D. C., "Simulation of Transition with a Two-Equation Turbulence Model," *AIAA Journal*, Vol. 32, No. 2, Feb. 1994, pp. 247–255.

[20] Warren, E. S., and Hassan, H. A., "An Alternative to the e^N Method for Determining Onset Transition," 35th AIAA Aerospace Sciences and Exhibit, Reno, NV, AIAA Paper 97-0825, Jan. 1997.

[21] Langtry, R. B., and Menter, F. R., "Transition Modeling for General CFD Applications in Aeronautics," 43rd AIAA Aerospace Sciences and Exhibit, Reno, NV, AIAA Paper 2005-522, Jan. 2005.

[22] Krimmelbein, N., Radespiel, R., and Nebel, C., "Numerical Aspects of Transition Prediction for Three-Dimensional Configurations," 35th AIAA Fluid Dynamics Conference and Exhibit, Toronto, AIAA Paper 2005-4764, June 2005.

[23] Arthur, M. T., Dol, H. S., Krumbein, A., Ponsin, J., and Houdeville, R., "Application of Transition Criteria in Navier–Stokes Computations," Group for Aeronautical Research and Technology in Europe TP-138, Jan. 2003.

[24] Stock, H. W., "Infinite Swept-Wing Navier–Stokes Computations with e^N Transition Prediction," *AIAA Journal*, Vol. 43, No 6, June 2005, pp 1221–1229. doi:10.2514/1.12487

[25] Krumbein, A., "Automatic Transition Prediction and Application to Three-Dimensional Wing Configurations," *Journal of Aircraft*, Vol. 44, No. 1, Jan.–Feb. 2007, pp. 119–133. doi:10.2514/1.22254

[26] Perraud, J., Séraudie, A., and Moens, F., "Transition on a High-Lift Swept Wing in the European Project EUROLIFT," *Journal of Aircraft*, Vol. 41, No 5, Sept. 2004, pp. 1183–1190. doi:10.2514/1.4297

[27] Kaups, K., and Cebeci, T., "Compressible Laminar Boundary Layers with Suction on Swept and Tapered Wings," *Journal of Aircraft*, Vol. 14, No 7, July 1977, pp. 661–667.

[28] Schrauf, G., "A Note on the Calculation of the Effective Sweep Angle and the Attachment Line Reynolds Number," Messerschmitt-Bolkow-Blohm TR TE 2-1636, Bremen, Germany, 1988.

[29] Perraud, J., "Transition Prediction for High Lift Applications, Implementation of Database Method in Boundary Layer Codes and Preliminary Validation," ONERA EUROLIFT TR 2.3-1, Toulouse, France, Jan. 2001.

[30] Krumbein, A., Stock, H. W., "Laminar-Turbulent Transition Modeling in Navier–Stokes Solvers Using Engineering Methods," *European Congress on Computational Methods in Applied Sciences and Engineering (ECCOMAS 2000)* [CD-ROM], International Center for Numerical Methods in Engineering, Barcelona, Sept. 2000.

[31] Rudnik, R., and Germain, E., "Re-No Scaling Effects on the EUROLIFT High-Lift Configurations," 45th AIAA Aerospace Sciences Meeting and Exhibit, Reno, NV, AIAA Paper 2007-752, Jan. 2007.